AGU PUBLICATIONS

JGR

Journal of Geophysical Research: Atmospheres

RESEARCH ARTICLE

10.1002/2016JD026266

Key Points:
- Modeling results suggest that 2012 elevated O_3 at surface sites is associated with increased exposure to upper troposphere and lower stratosphere
- In spring 72% and summer 65% of O_3 vertical profiles have elevated O_3 lamina (3-8 km, $O_3 > 70$ ppb)
- Observational analysis highlights importance of both surface O_3 and O_3 aloft in understanding the varying sources of O_3 in the western U.S.

Supporting Information:
- Supporting Information S1
- Figure S1
- Figure S2
- Figure S3
- Figure S4

Correspondence to:
E. L. Yates,
emma.l.yates@nasa.gov

Citation:
Yates, E. L., Johnson, M. S., Iraci, L. T., Ryoo, J.-M., Pierce, R. B., Cullis, P. D., … Tanaka, T. (2017). An assessment of ground level and free tropospheric ozone over California and Nevada. *Journal of Geophysical Research: Atmospheres*, *122*. https://doi.org/10.1002/2016JD026266

Received 17 NOV 2016
Accepted 28 AUG 2017
Accepted article online 31 AUG 2017

An Assessment of Ground Level and Free Tropospheric Ozone Over California and Nevada

E. L. Yates[1], M. S. Johnson[2], L. T. Iraci[1], J.-M. Ryoo[1], R. B. Pierce[3], P. D. Cullis[4], W. Gore[1], M. A. Ives[5], B. J. Johnson[6], T. Leblanc[7], J. E. Marrero[1], C. W. Sterling[4], and T. Tanaka[1]

[1]Atmospheric Science Branch, NASA Ames Research Center, Mountain View, CA, USA, [2]Biospheric Science Branch, NASA Ames Research Center, Mountain View, CA, USA, [3]NOAA/NESDIS Advanced Satellite Products Branch Madison, Madison, WI, USA, [4]Cooperative Institute for Research in Environmental Sciences, University of Colorado Boulder, Boulder, CO, USA, [5]Trinidad Head Observatory, ESRL, NOAA, Trinidad Head, CA, USA, [6]Global Monitoring Division, NOAA Earth System Research Laboratory, Boulder, CO, USA, [7]Jet Propulsion Laboratory, Table Mountain Facility, California Institute of Technology, Wrightwood, CA, USA

Abstract Increasing free tropospheric ozone (O_3), combined with the high elevation and often deep boundary layers at western U.S. surface stations, poses challenges in attaining the more stringent 70 ppb O_3 National Ambient Air Quality Standard. As such, use of observational data to identify sources and mechanisms that contribute to surface O_3 is increasingly important. This work analyzes surface and vertical O_3 observations over California and Nevada from 1995 to 2015. Over this period, the number of high O_3 events (95th percentile) at the U.S. Environmental Protection Agency Clean Air Status and Trends Network (CASTNET) sites has decreased during summer, as a result of decreasing U.S. emissions. In contrast, an increase in springtime 5th percentile O_3 indicates a general increase of baseline O_3. During 2012 there was a peak in exceedances and in the average spring-summer O_3 mixing ratios at CASTNET sites. Goddard Earth Observing System-Chem results show that the surface O_3 attributable to transport from the upper troposphere and stratosphere was increased in 2013 compared to 2012, highlighting the importance of measurements aloft. Vertical O_3 measurements from aircraft, ozonesondes, and lidar show distinct seasonal trends, with a high percentage of elevated O_3 laminae ($O_3 > 70$ ppb, 3–8 km) during spring and summer. Analysis of the timing of high O_3 surface events and correlation between surface and vertical O_3 data is used to discuss varying sources of western U.S. surface O_3.

1. Introduction

Boundary layer ozone (O_3) is a secondary pollutant formed through photochemical reactions involving nitrogen oxides (NO_x), carbon monoxide (CO), and volatile organic compounds (VOCs). It is destroyed by dry deposition at the surface and through reactions involving water and O_3 photolysis, leading to the production of the hydroxyl radical (OH) (Parrish et al., 2012). O_3 can be transported to the boundary layer from the stratosphere where it is present in large quantities (e.g., Langford et al., 2017, 2012, 2015; Lin et al., 2012; Yates et al., 2013). The lifetime of boundary layer O_3 is a few days, whereas in the free troposphere it is several weeks and as such O_3 can be transported in the free troposphere on intercontinental scales (Zhang et al., 2008). In the western U.S., enhanced free tropospheric O_3 due to Asian pollution has been frequently observed during spring (e.g., Ambrose et al., 2011; Langford et al., 2015; Ryoo et al., 2017) and models estimate that Asian O_3 can provide 5–15 ppb of additional O_3 to surface sites during trans-Pacific transport events (Brown-Steiner & Hess, 2011; Lin et al., 2012, 2017).

The U.S. Environmental Protection Agency (EPA) defines the current National Ambient Air Quality Standards (NAAQS) for O_3 as 70 parts per billion by volume (ppbv). A location is in violation of the O_3 NAAQS when the 3 year average of the fourth highest daily maximum 8 h average O_3 (MDA8) exceeds this 70 ppbv threshold. The recent reduction of the O_3 MDA8 from 75 to 70 ppb (U.S. Environmental Protection Agency) will likely have significant consequences for many surface O_3 sites in the western U.S. In the western U.S. the free tropospheric baseline has risen in recent years as a result of rising Asian emissions (Cooper et al., 2010; Gratz et al., 2015; Lin et al., 2012, 2017; Zhang et al., 2010), deep stratospheric intrusions (Langford et al., 2012; Lefohn et al., 2011; Lin et al., 2015) and more frequent wildfires (Jaffe, 2011; Jaffe & Widger, 2012). High surface elevation and often deep atmospheric boundary layers, which aid

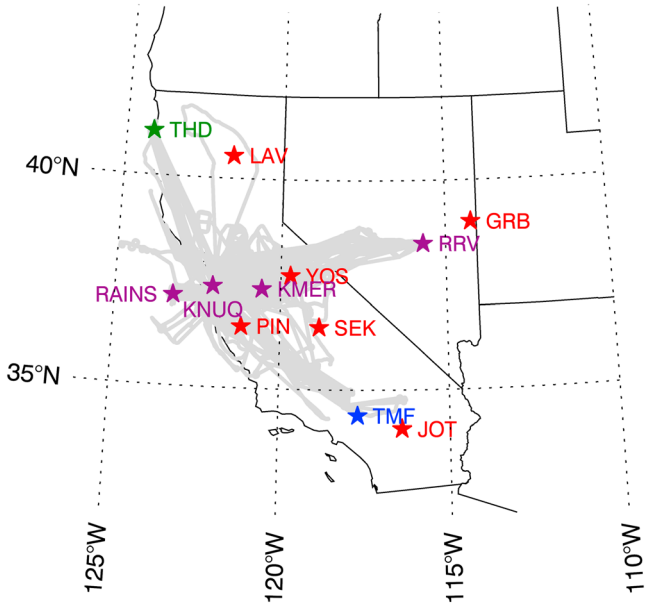

Figure 1. Map of selected O_3 CASTNET sites (red) in California and Nevada. Great Basin (GRB, elev. 2,060 m), Joshua Tree (JOT, elev. 1224 m), Lassen Volcanic (LAV, elev. 1,756 m), Pinnacles (PIN, elev. 335 m), Sequoia (SEK, elev. 1,225 m), Yosemite (YOS, elev. 1605 m) National Parks. Also indicated are the location of the NOAA Trinidad Head (THD, green) ozonesonde site, JPL Table Mountain Facility (TMF, blue), locations of common AJAX profile sites (purple): Castle Airport, Merced (KMER), Railroad Valley, NV (RRV), offshore (RAINS) and Moffett Field (KNUQ), and AJAX flight tracks from 148 flights analyzed in this study (gray lines).

mixing with the free troposphere, make many western U.S. surface sites more susceptible to influences from increasing baseline ozone and increasing temperatures (Jaffe & Zhang, 2017), posing challenges in attaining the more stringent NAAQS and increasing the probability of O_3 nonattainment outside of the typical photochemical O_3 summertime season (Cooper et al., 2015).

With the reduction in the NAAQS, identifying various sources and transport mechanisms that contribute to surface O_3 will be increasingly important to determine the regulatory policies required for attainment (Cooper et al., 2015). Despite these concerns, O_3 observations in the remote western U.S. are sparse, with recent research highlighting deficiencies in the current observation network to accurately detect interannual variability of O_3 (Lin et al., 2015). Our study compiles 4 years of tropospheric O_3 vertical profiles over California and Nevada measured by aircraft, ozonesonde, and lidar to analyze the occurrence of elevated O_3 layers. We also assess longer-term O_3 trends at rural surface sites and model the impacts of elevated O_3 layers aloft on surface values, using existing observations.

Here we analyze vertical profiles of O_3 from the Alpha Jet Atmospheric eXperiment (AJAX) over California and Nevada (34–41°N and 115–123°W), ozonesondes launched from Trinidad Head, CA (THD, 41.0541°N, 124.151°W), and tropospheric ozone profiles from the differential absorption lidar (DIAL) situated at the JPL Table Mountain Facility, CA (TMF, 34.3820°N, 117.6818°W). Surface O_3 from the U.S. EPA Clean Air Status and Trends Network (CASTNET) is used to discuss surface trends. Goddard Earth Observing System (GEOS)-Chem is used to determine the trends in regional O_3 and assesses the contributions of various sources on surface O_3. Specifically, we address the following questions:

1. How does the lowered NAAQS impact the frequency and timing of surface O_3 violations?
2. Do we observe elevated O_3 during 2012 at surface sites as reported in previous studies (Baylon et al., 2016; Lin et al., 2015)? And if so, what are the causes?
3. How variable is free tropospheric O_3 over California and Nevada?
4. How can O_3 observational data be used to assess the sources of surface O_3?

2. Methods

2.1. Surface O_3 Measurements

Rural surface measurements from six O_3 sites in California and Nevada were obtained from CASTNET (https://www.epa.gov/castnet). Figure 1 shows a map of the CASTNET sites used in this analysis including Great Basin (GRB) National Park in Nevada and Joshua Tree (JOT), Lassen Volcanic (LAV), Pinnacles (PIN), Sequoia (SEK), and Yosemite (YOS) National Parks in California.

2.2. Free Tropospheric O_3 Measurements

In situ O_3 is measured on board the AJAX platform using a commercial O_3 monitor (2B Technologies Inc., model 205) based on ultraviolet absorption techniques and modified for flight worthiness. Details of the modification, calibration, and sampling system are reported by Yates et al. (2013). Overall accuracy of the O_3 instrument is determined to be 3 ppb.

From January 2011 to January 2016 a total of 148 flights was flown over California and Nevada with 49 in spring (April to June), 35 in summer (July to September), 30 in fall (October to December), and 34 in winter (January to March). It should be noted that although in most flights meteorological conditions are considered random, all of the flights are conducted under conditions avoiding aircraft icing, i.e., clouds are avoided, as

are days with heavy precipitation. Some flights are targeted for specific synoptic conditions, for example, clear-sky conditions or upper atmospheric disturbances, which may introduce some bias to this data set. A map of AJAX flight tracks used during this study is presented in Figure 1.

Vertical profiles from 212 ozonesondes launched from THD between January 2011 and January 2016 are used in this analysis. A thorough description of the NOAA baseline station at Trinidad Head and O_3 profile measurements by standard electrochemical (electrochemical concentration cell) ozonesondes is presented by Oltmans et al. (2008, and references therein). Ozonesonde data were downloaded from ftp://aftp.cmdl.noaa.gov/data/ozwv/Ozonesonde/. About 388 tropospheric O_3 profiles from January 2011 to July 2015 from the DIAL lidar at TMF, which is part of the Tropospheric Ozone Lidar NETwork, are also analyzed. Lidar data were downloaded from ftp://ftp.cpc.ncep.noaa.gov/ndacc/station/. Details on the DIAL system are provided by McDermid et al. (2002).

2.3. GEOS-Chem Model Description

The global 3-D chemical transport model GEOS-Chem (v9–02; http://geos-chem.org/), with the modifications described in Travis et al. (2016), was applied during this study to simulate emissions, atmospheric chemistry, and transport of O_3 and its precursor species. The model is driven by data-assimilated meteorological fields from the Goddard Earth Observing System version 5 FP (GEOS 5 FP) from the National Aeronautics and Space Administration (NASA) Global Modeling Assimilation Office (Bey et al., 2001). The model applied a horizontal resolution of 2.0° × 2.5° (latitude × longitude) and 47 vertical hybrid sigma pressure levels from the surface up to ~80 km above ground level (agl) (~0.01 hPa). The model has relatively high vertical resolution near the surface with 14 vertical grids on average in the bottom 2 km agl, and the first vertical grid has a resolution of ~100 m. Aerosol and gaseous species transport is calculated every 15 min in the model following the scheme described in Lin and Rood (1996). Atmospheric chemistry calculations in the model include an O_3-NO_x-hydrocarbon-aerosol mechanism coupled to H_2SO_4-HNO_3-NH_3 aerosol thermodynamics (Bey et al., 2001). GEOS-Chem simulates planetary boundary layer (PBL) mixing following the work by Lin and McElroy (2010) and takes into account the magnitude of atmospheric instability. Dry deposition predictions are based on the resistance in series scheme described in Wang et al. (1998), and wet deposition calculations apply the methods of Liu et al. (2001) for aerosols and Amos et al. (2012) for gases. GEOS-Chem calculates stratospheric O_3 formation using the Linoz linearized parameterization above the GEOS 5 dynamic tropopause (McLinden et al., 2000), and this O_3 is then transported to the troposphere using modeled winds. Another important source of O_3 is trace gases from wildfires and the model treats daily biomass burning emissions using the Quick Fire Emissions Data set emissions database (Darmenov & da Silva, 2015).

To track individual sources of O_3, global tagged tracer simulations of GEOS-Chem were conducted for May–September 2012 and May–September 2013 at a 2° × 2.5° resolution. Note that, due to GEOS 5 FP meteorological data availability and model spin-up times, April was excluded from the GEOS-Chem analysis. Full chemistry GEOS-Chem simulations provide 3-D production and loss (P/L) rates of O_3 for every time step to be applied in tagged tracer simulations. The individual tagged O_3 tracer sources simulated during this study are (1) total, (2) stratosphere, (3) upper troposphere, (4) middle troposphere, (5) Pacific Ocean boundary layer (BL), (6) North America (NA) BL, (7) Atlantic Ocean BL, (8) Europe BL, (9) Africa BL, (10) Asia BL, and the (11) rest of the world (encompassing all 3-D regions not specified in other tagged tracers). The primary analysis during this study focused on upper tropospheric and stratospheric source (UT/S), Asia BL, and NA BL. These sources were chosen to evaluate the impact of long range transport, stratosphere-to-troposphere transport, and local O_3 production on surface air quality in the western U.S. The concentration of each tagged O_3 tracer is calculated using the full-chemistry model-predicted P/L rates which occur in the geographic region defined for each source. During this study, stratospheric O_3 is defined as all O_3 formed above the GEOS 5 FP dynamic tropopause; upper tropospheric O_3 is assumed to be from the tropopause to ~350 hPa, Asia BL is defined as all O_3 formed below the GEOS 5 FP PBL height north of 10°S and between 55°E and 150°E, and NA BL is defined as all O_3 formed below the GEOS 5 FP PBL height north of 15°N and between 127.5°W and 65°W. Upon production within the specific geographical region, the individual tracers are transported separately and are subjected to chemical loss rates and deposition processes globally.

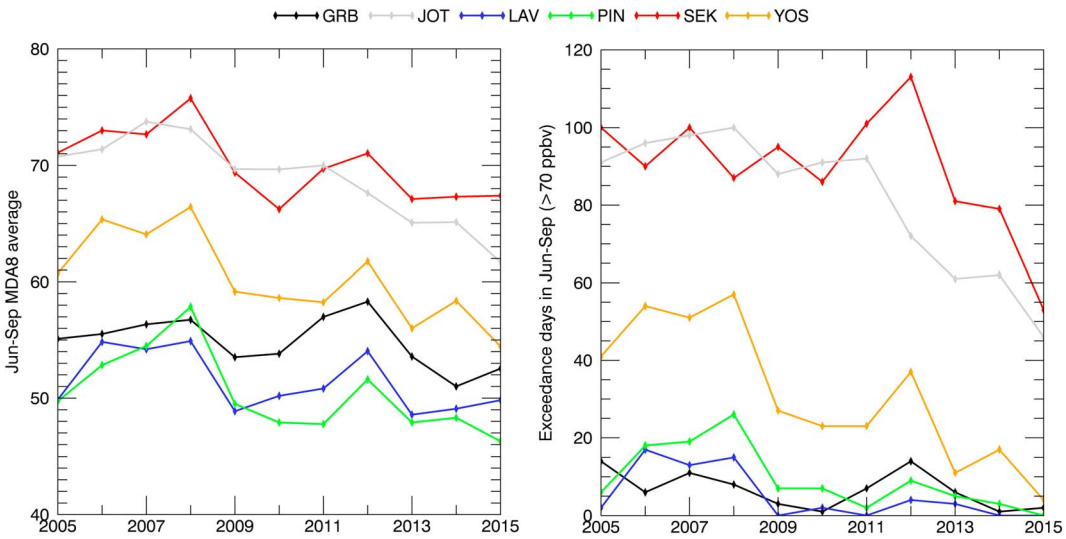

Figure 2. (left) April–September average MDA8 O_3 during 2005–2015 and (right) number of exceedance days in April–September (MDA8 > 70 ppb) at Great Basin (GRB, black), Joshua Tree (JOT, gray), Lassen Volcanic (LAV, blue), Pinnacles (PIN, green), Sequoia (SEK, red), and Yosemite (YOS, orange) National Parks.

3. Results and Discussions

3.1. Baseline O_3 Surface Site Observations

Figure 2 (left) presents the interannual variability in MDA8 O_3 for six CASTNET sites for April–September 2005 to 2015. The average April–September MDA8 O_3 in 2015 ranges between 46 ppb at PIN and 67 ppb at SEK. SEK and JOT, followed by YOS, consistently have the highest MDA8 O_3. These sites, although considered rural for CASTNET measurement purposes, are frequently influenced by anthropogenic emissions from large urban areas (Burley et al., 2014; Burley & Ray, 2007; Bytnerowicz et al., 2002; Cooper et al., 2012; Lin et al., 2017; VanCuren, 2015). During 2005–2015, the total number of days the MDA8 exceeded 70 ppb during April–September ranges from 113 days at SEK in 2012 to 0 days in LAV in 2009, 2011, 2014–2015 and 0 days at PIN in 2015 (Figure 2, right).

Table 1
The 1995–2015 O_3 MDA8 Rate of Change as Determined by the Slope of Linear Regression (ppb/year) in the 5th, 50th, and 95th Percentiles for April–May and June–September

	5th	50th	95th
GRB O_3: Jun–Sep	0.06 (0.53)	−0.06 (0.52)	−0.20 (0.10)
GRB O_3: Apr–May	0.19 (0.06)	**0.28 (0.05)**	0.11 (0.44)
JOT O_3: Jun–Sep	0.04 (0.80)	−0.27 (0.06)	**−0.88 (0.00)**
JOT O_3: Apr–May[a]	**0.09 (0.02)**	0.03 (0.67)	**−0.54 (0.02)**
LAV O_3: Jun–Sep	0.02 (0.82)	−0.08 (0.38)	**−0.47 (0.01)**
LAV O_3: Apr–May	0.17 (0.14)	**0.17 (0.05)**	0.03 (0.84)
PIN O_3: Jun–Sep	**−0.27 (0.01)**	**−0.60 (<0.01)**	**−0.87 (<0.01)**
PIN O_3: Apr–May	0.05 (0.78)	−0.11 (0.34)	−0.26 (0.18)
SEK O_3: Jun–Sep[b]	−0.11 (0.69)	**−0.41 (0.03)**	**−0.72 (0.01)**
SEK O_3: Apr–May[c]	0.05 (0.85)	−0.23 (0.50)	−0.76 (0.06)
YOS O_3: Jun–Sep	−0.09 (0.61)	**−0.40 (0.02)**	**−0.72 (<0.01)**
YOS O_3: Apr–May	−0.01 (0.09)	0.18 (0.19)	0.01 (0.95)

Note. The correlation *p* value is reported in parentheses. Red indicates positive trends, blue indicates negative trends, and bold text highlights statistically significant trends.
[a]Excludes 2001 data. [b]Excludes 1997, 1998, and 2004. [c]Excludes 1995–2000 and 2004.

Figure 2 shows an apparent decreasing trend in the average O_3 MDA8 and number of exceedance days between 2005 and 2015 at the more polluted sites (JOT, SEK, and YOS) which is not evident at the cleaner sites (GRB, LAV, and PIN). An analysis of the longer-term spring (April–May) and summer (June–September) MDA8 O_3 trends between 1995 and 2015 is presented in Table 1 and Figures S1 and S2 in the supporting information. The O_3 rate of change (ppb per year) over 1995 to 2015 was calculated for low, middle, and high O_3 events, from the linear fit through the 5th, 50th, and 95th percentiles, respectively, of the MDA8 O_3 during spring and summer data at each site. The goodness of fit of the linear regression was determined using the standard *F* statistic and associated *p* value to determine its significance. The null hypothesis is that O_3 does not vary with time (years); hence, if the associated *p* value was small ($p \leq 0.05$), the variability of O_3 with time is assumed to be statistically significant.

The summer (June–September) 1995–2015 O_3 slope is negative and statistically significant at the 95th percentile for all sites except GRB, ranging from −0.47 to −0.88 ppb yr^{-1} PIN, JOT, SEK, and YOS show the largest negative slopes at the 95th percentile, indicating the reduced frequency of extreme O_3 events. PIN is one of the less-polluted sites, yet its large negative slope suggests that it is

influenced by large urban areas within ~100 km (San José/Santa Clara County and San Joaquin Valley). Cooper et al. (2012) and Lin et al. (2017) also reported negative trends at the 95th percentile for JOT, LAV, PIN, and SEK during summer, 1990–2010 (Cooper et al., 2012) and 1988–2014 (Lin et al., 2017). At the 50th percentile, all slopes are again negative with three sites in central California (PIN, SEK, and YOS) statistically significant. More variability is seen at the 5th percentile. Three sites (GRB, JOT, and LAV) show increases, and three (PIN, SEK, and YOS) show decreases, but only PIN is significant. This increased variability among surface sites in the 5th and 50th percentiles are also reported by Cooper et al. (2012) and Lin et al. (2017).

For comparison with previous studies which report increasing springtime O_3 in the western U.S. (e.g., Cooper et al., 2012; Langford et al., 2015; Lin et al., 2012, 2017), we also consider the O_3 rate of change for spring (April–May) 1995–2015 in Table 1. Overall, there are fewer significant trends in spring than summer, with only JOT showing a significant decrease at the 95th percentile, one significant increase at the 50th percentile (LAV) and one significant increase at the 5th percentile (JOT). The analysis presented here expands on work by Cooper et al. (2012), updating the trend analysis to include more recent years but for a selected number of western U.S. surface O_3 sites. Overall in spring, there are more increases than decreases in O_3 trends indicating a general O_3 increase despite decreasing U.S. O_3-precursor emissions. The general increase of springtime low O_3 events (5th percentile) has been linked to increasing baseline O_3 in the western U.S. (Cooper et al., 2012; Lin et al., 2017). In contrast, in summer there are more overall decreases than there are increases, indicating that U.S. anthropogenic emission reductions are decreasing summertime O_3 in the western U.S.

Another feature evident in Figure 2 is that the average April–September MDA8 O_3 (Figure 2, left) and number of exceedance days (Figure 2, right) are notably enhanced during 2008 and 2012 at most sites. The 2008 and 2012 enhancements are also evident in springtime only (April–May) MDA8 O_3 (data not shown); modelling results by Lin et al. (2015) suggest that larger springtime surface O_3 values in the western U.S. during 2008 and 2012 were due to stronger stratospheric folding events occurring following strong La Niña winters. Years 2008 and 2012 were also particularly active wildfire years (CAL FIRE, 2017, http://www.fire.ca.gov/fire_protection/fire_protection_fire_info_redbooks, accessed 1 April 2017), which may also contribute to the increased ozone amounts; however, there are large uncertainties about the rate of O_3 production within wildfire plumes. Reports range from O_3 depletion to substantial formation (e.g., Akagi et al., 2013; Jaffe & Widger, 2012; Pfister et al., 2008; Singh et al., 2012; Yates et al., 2016).

We quantified the 2012 increase by averaging the April–September MDA8 O_3 value at each site for the two years before and after 2012 and subtracting from the 2012 April–September average. The 2012 increase ranged from 3.4 ppb at SEK to 4.5 ppb at GRB; this is equivalent to an increase of 5.1–8.8%. JOT, one of the sites most influenced by urban emissions, showed distinctly different behaviors, with only 0.2 ppb increase in 2012. Previous observation-based analyses have reported a springtime increase in MDA8 O_3 at U.S. surface sites in the Pacific northwest (Baylon et al., 2016; Fine et al., 2014) associated with an influx of O_3 from the UT/S (Baylon et al., 2016; Lin et al., 2015). The increases reported in this study fall inside the range of those reported by Baylon et al. (2016).

To explore the cause of the 2012 increase, we utilized GEOS-Chem in a tagged O_3 tracer mode. The daytime-averaged (11 am to 6 pm) surface level May–September O_3 during 2012 and 2013 from three major O_3 sources (UT/S, long-range transport from Asia boundary layer (BL), and North America (NA) BL) is shown at each analyzed CASTNET site in Figure 3. The daytime averaged values were chosen for evaluation to better correspond with higher O_3 concentrations which typically occur during the afternoon. The differences (2012 minus 2013) in total O_3 at each site ranged between 1 and 3 ppb. The largest differences were seen at GRB, LAV, and YOS, the three highest elevation sites analyzed in this study. Of the three sources examined, UT/S sources of O_3 have the largest magnitude and also the largest differences between 2012 and 2013 (from 1.1 ppb at PIN to 2.6 ppb at GRB), with the largest differences being at the higher elevation sites.

North America boundary layer O_3 sources also display somewhat higher values in 2012 compared to 2013 (from 0.2 ppb at JOT to 1.2 ppb at PIN). NA O_3 sources include all O_3 formed in the boundary layer over NA and are most likely associated with trace gas emissions from local sources including wildfire emissions.

Asian BL sources have minimal differences between the two years (differences range from −0.1 to 0.2 ppb). Note that the prediction of the impact of emissions in Asia on O_3 in the western U.S. in this study is likely a

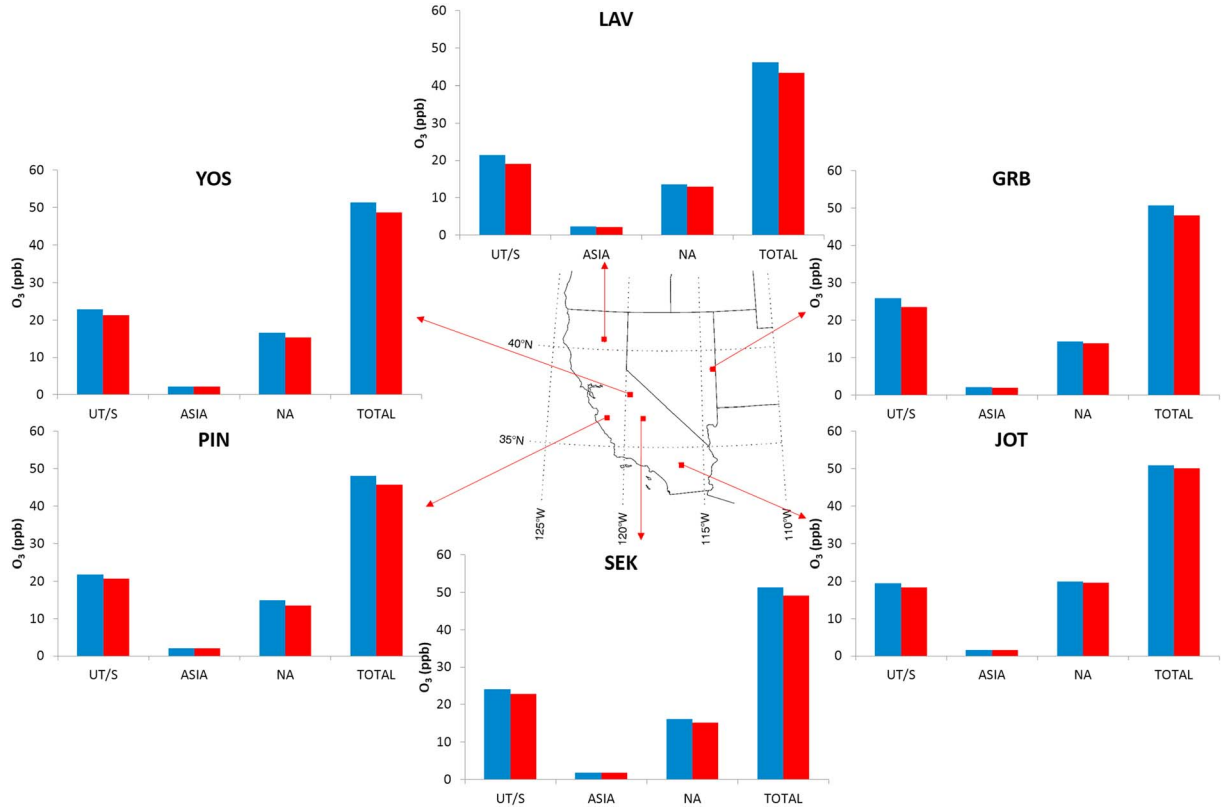

Figure 3. Results from GEOS-Chem tagged O_3 tracer simulation at the location of CASTNET stations evaluated during this study (Great Basin (GRB), Joshua Tree (JOT), Lassen Volcanic (LAV), Pinnacles (PIN), Sequoia (SEK), and Yosemite (YOS) National Parks). The daytime-averaged (ppb) surface mixing ratios between May and September from the main O_3 sources: UT/S (Upper Troposphere and Stratosphere), ASIA (boundary layer), and NA (North America boundary layer) and total O_3 during 2012 (blue bars) and 2013 (red bars).

lower bound estimate, as it only presents the O_3 formed in the BL over the Asian continent and transported to NA, not O_3 formed during transport.

Overall, the tagged O_3 tracer simulation suggests that O_3 associated with the UT/S was noticeably enhanced at the surface in the western U.S. during 2012 compared to 2013 and could be contributing to the larger number of exceedance days experienced at the CASTNET sites. The model results from this simulation agree with recent studies which have demonstrated that UT/S O_3 was larger in the western U.S. during May 2012 (Baylon et al., 2016; Lin et al., 2015). Additionally, we find increases in UT/S O_3 (up to 5 ppb) during all months of 2012 except July, compared to 2013, indicating that UT/S O_3 can play a large role lasting throughout spring and summer months.

Figure S3 shows the regional observed and simulated monthly mean O_3, averaged over the six CASTNET sites. GEOS-Chem underpredicts the regional monthly mean observed values in May–June by 7 ppb and overestimates in July–August by a few ppb. In late summer (September) GEOS-Chem agreed well with observations. Previous studies have shown a similar level of agreement, for example, Fiore et al. (2003) reported that GEOS-Chem generally falls within 5 ppb of the regional mean observed values at CASTNET sites located within the northwest and southwest U.S.

In the context of the recent tightening of the NAAQS and the continued observation of increasing baseline O_3, it is important to understand the changes to surface O_3 exceedances in the rural, western U.S. Figure 4 presents a comparison of the number of O_3 exceedances of the old (75 ppb) and new (70 ppb) NAAQS. At all surface sites, as can be expected, the number of O_3 exceedances increases as the NAAQS is lowered from 75 to 70 ppb, with annual increases in the number of additional exceedances as high as 38 days seen at JOT during 2010–2011 (see Figure 4, right). The most polluted sites (JOT, SEK, and YOS) show the largest increases in the number of exceedance days. A monthly breakdown of the impact of tightening the NAAQS on the total number of exceedances is shown in Figure 4 (left). The majority of additional exceedance days as a result of

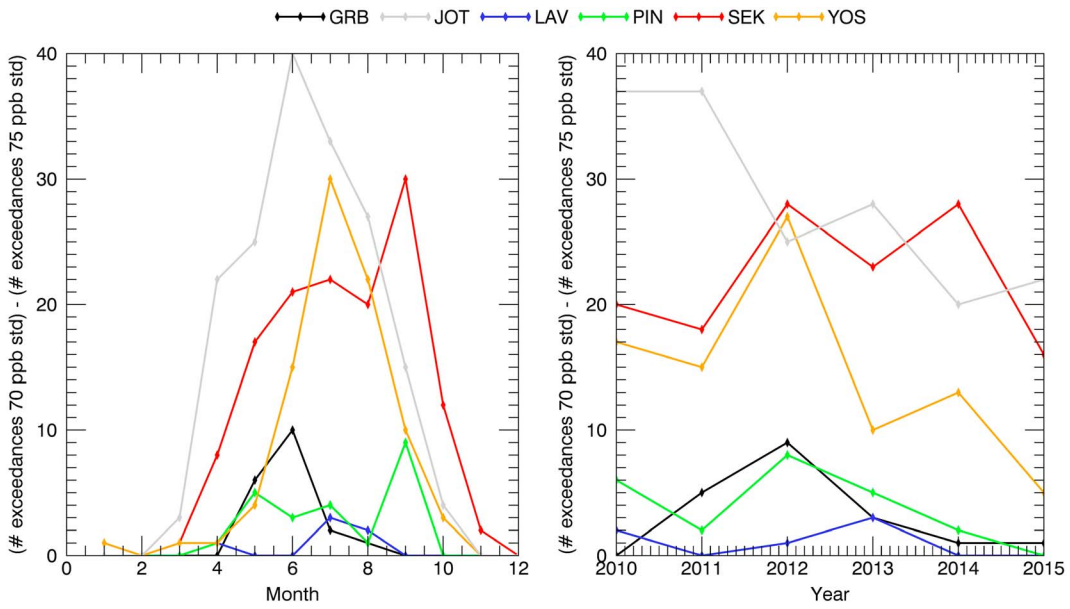

Figure 4. Assessing the impact of the reduced NAAQS on the number of O_3 exceedances during 2010–2015 by (left) month and (right) year at Great Basin (GRB, black), Joshua Tree (JOT, gray), Lassen Volcanic (LAV, blue), Pinnacles (PIN, green), Sequoia (SEK, red), and Yosemite (YOS, orange) National Parks (the total number of exceedances of 70 ppb standard minus the total number of exceedances of 75 ppb standard for 2010–2015).

the lowered NAAQS fall within summer months, but exceedances also start to appear in spring and fall. Thus, the reduction of the NAAQS has direct impacts, significantly increasing the number of exceedance days that would have occurred during 2010–2015 in summer as well as causing exceedances in spring and winter/fall. This observation will have direct consequences on the ability of the western U.S. to meet the tightened NAAQS without further reductions in anthropogenic emissions, especially within the context of increasing baseline O_3.

3.2. Free Tropospheric O_3 Observations

O_3 increases as a function of altitude, and so the high elevation terrain of much of the western U.S. is exposed to increased O_3 levels (Jaffe & Zhang, 2017). As such, understanding the trends of O_3 aloft is an important factor in understanding surface O_3 in the western U.S. A seasonal and vertical summary of O_3 observations is presented in Figure 5. In all seasons, the mean O_3 profiles (bold colored lines) show a positive vertical gradient between the boundary layer and free troposphere (e.g., compare average O_3 at 0.5 and 3 km in Figure 5) as presented in previous studies (e.g., Brodin et al., 2010; Jaffe, 2011; Newchurch et al., 2003; Parrish et al., 2010; Pfister et al., 2011). Generally, there is good agreement between the seasonal mean O_3 from different observation methods, despite differences in measurement location, instrumentation, date, and time. Agreements are typically within 10 ppb but with increased variance at higher altitudes and within the summertime boundary layer.

The spread of all measured O_3 (gray lines) for each season is also shown in Figure 5. Spring and summer exhibit increased variability of free tropospheric O_3, with thin layers (laminae) of high O_3 concentrations ($>$ 70 ppb) regularly observed, which are not commonly observed in fall and winter. In spring 72% and summer 65% of O_3 profiles (AJAX, ozonesondes, and lidar) have high O_3 lamina, defined as $O_3 > 70$ ppbv between 3 and 8 km, compared to only 15% in fall and 22% in winter. The frequency and magnitude of O_3 laminae observed during spring and summer show that high O_3 in the free troposphere is a regular occurrence. Observation of O_3 laminae, correct identification of the sources (local or long-range transported pollution or upper troposphere lower stratosphere (UTLS)), and potential impacts on surface O_3 are of importance from a regulatory perspective in the context of increasing baseline O_3 and more stringent air quality standards. The composite monthly mean O_3 mixing ratios from each data set (aircraft, ozonesonde, and lidar) is presented in Figure S4, illustrating how elevated O_3 extends to lower altitudes during spring/summer

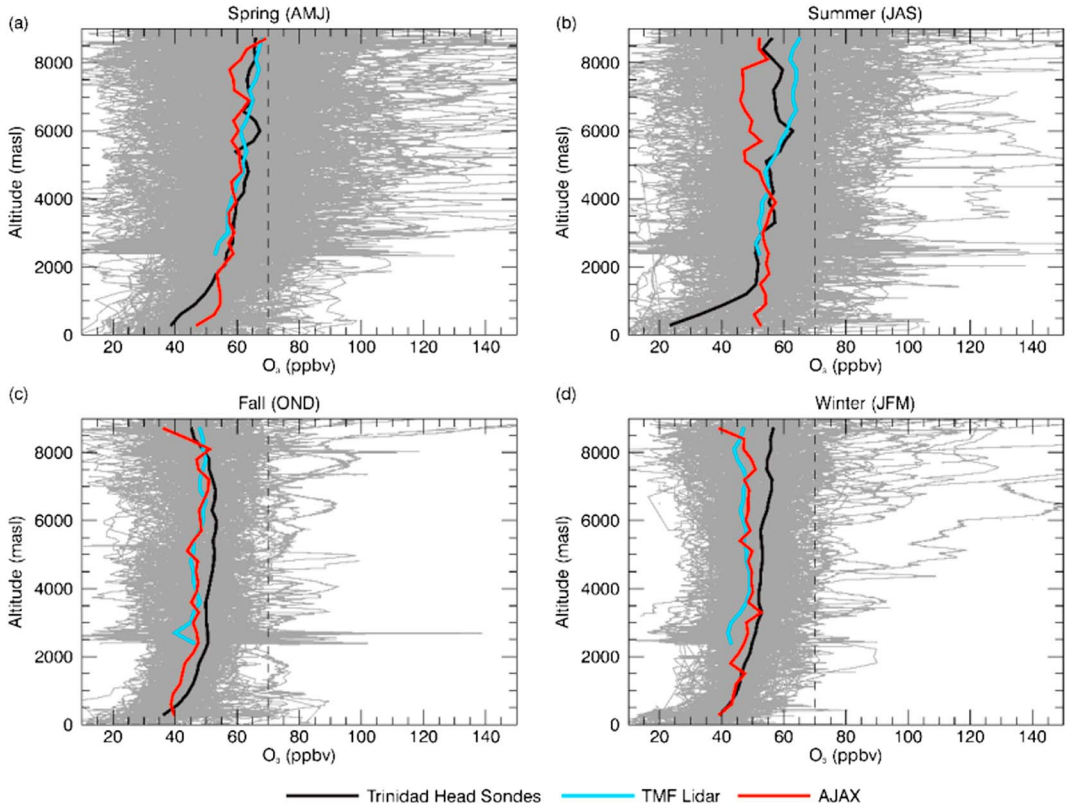

Figure 5. Seasonal O_3 profiles (January 2011 to December 2015) during (a) spring (April, May, June (AMJ)), (b) summer (July, August, September (JAS)), (c) fall (October, November, December (OND)), and (d) winter (January, February, March (JFM)). Bold lines highlight the seasonal averages from aircraft (AJAX, red), ozonesonde (Trinidad Head, black), and the lidar (Table Mountain, blue). The black dashed vertical lines indicate the 70 ppbv NAAQS. The gray lines present all O_3 data measured by AJAX, ozonesonde, and lidar (Note: Lidar data cover January 2012 to July 2015).

than fall/winter. In the AJAX and ozonesonde data sets, a monthly mean $O_3 > 60$ ppb is generally found above 3 km (above 4 km in lidar data) during spring and summer.

Figure 6 compares the monthly mean trends averaged over different altitude slices. Figure 6 (top) presents the mean seasonal O_3 cycle from combined measurements by aircraft, ozonesondes, and lidar from January 2011 to May 2015. Over all altitudes (0–8 km, gray line) there is a broad O_3 maximum between March and August. The O_3 seasonal cycle data were filtered by altitude to better explore trends more representative of the boundary layer (<3 km, blue in Figure 6, top) and free troposphere (3–8 km, green). The combined O_3 seasonal cycle within the free troposphere follows a trend similar to the mean trend over all altitudes, with a maximum in April, indicating that free tropospheric measurements are driving the mean 0–8 km seasonal cycle. Dividing the free tropospheric observations by measurement type, each measurement data set (AJAX, ozonesonde, and lidar) shows an O_3 maximum in spring, with peaks between April and May (Figure 6, middle), coincident with the Northern Hemisphere maximum in cross-tropopause mass flux observed in late spring-summer (Appenzeller et al., 1996; Škerlak et al., 2014). Lidar data do show some bimodal variability, with a secondary peak in August. This is likely because the TMF lidar is at 2285 m above sea level, and the local (polluted) boundary layer often extends above 3 km, which means there will be some influence of anthropogenic emissions in the lidar 3–8 km range.

The boundary layer (<3 km) O_3 seasonal cycle is bimodal with peaks in May–June and August–September in AJAX and lidar data sets (Figure 6, bottom), indicative of the competing influences on boundary layer O_3 in the western U.S. The summertime O_3 maximum is generally associated with the peak in photochemical O_3 production, whereas the springtime maximum is attributed to the combination of enhanced stratosphere-to-troposphere transport, long-range transport of pollution, and photochemical production (Cooper et al.,

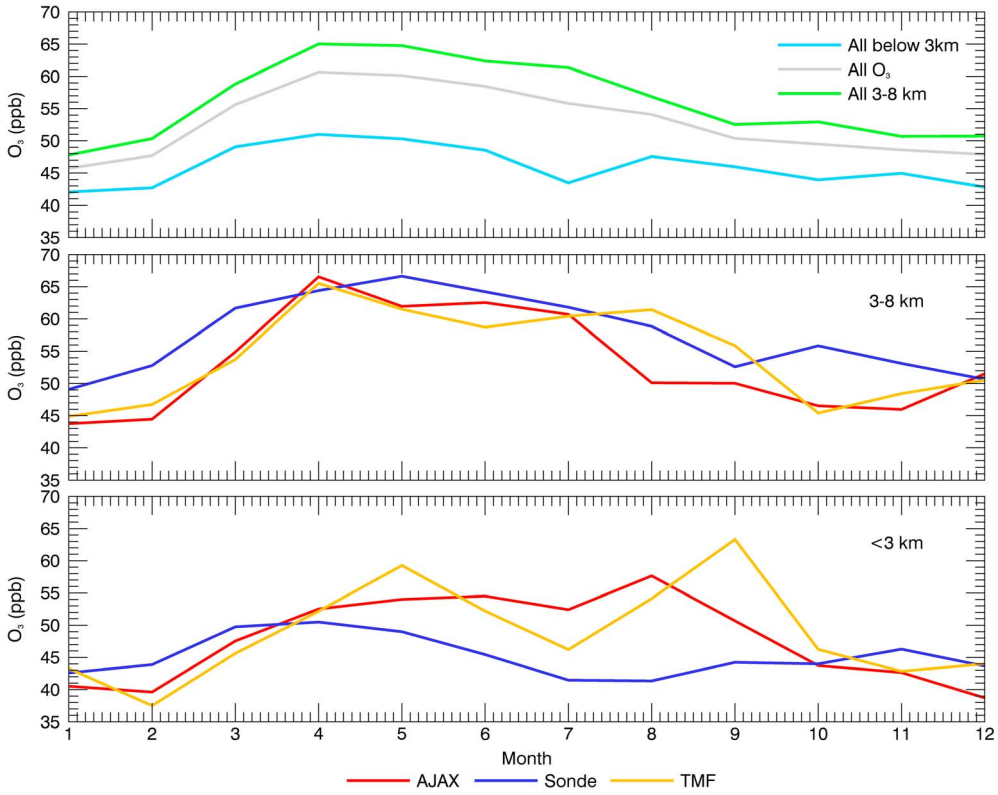

Figure 6. January 2011 to December 2015 averaged seasonal O_3 cycle of combined measurements by AJAX (red), ozonesonde (blue), and the tropospheric lidar (TMF, orange) at (middle) 3–8 km and (bottom) below 3 km. (top) The monthly averages of all the data from surface to 8 km (gray), between 3 and 8 km (green, free troposphere), and below 3 km (blue, boundary layer).

2011; Granados-Muñoz & Leblanc, 2016; Lin et al., 2012; Parrish et al., 2013). Variations in $O_3 < 3$ km observed by AJAX, THD ozonesonde, and lidar can be expected when considering differences in site location, timing of measurements, and variability of data density.

THD ozonesonde data <3 km are representative of the marine boundary layer and exhibit a spring maximum and summer minimum, in good agreement with surface O_3 trends reported at THD (Parrish et al., 2010). AJAX data <3 km are more representative of continental air masses. Typically in summertime AJAX will fly more boundary layer flights investigating O_3 exceedances in California's San Joaquin Valley than in wintertime, and as such AJAX data have a broad O_3 maximum during spring and summer (Jaffe, 2011). TMF lidar <3 km shows higher variability in monthly averages than AJAX and ozonesonde observations, with peaks in May and September. The higher variability may be due to the close proximity of the station to large anthropogenic sources from the Los Angeles basin, the elevation of the TMF site (2285 m), or the time of day of measurements. AJAX typically flies between 11:00 and 15:00; ozonesondes are typically launched at 11:00, and the TMF lidar profiles are typically between 19:00 and 00:00 local time. The similarities in the trends and relative orders of magnitudes of the monthly mean O_3 merits comparison, even with the caveats of the differences in location and timing.

3.3. Investigating O_3 Sources Using Temporally Resolved Observational Data

Figure 7 presents the timing of high-surface O_3 events (defined as occurrences of $O_3 > 70$ ppb) which may be used to distinguish between different O_3 sources. First, looking at the monthly distribution, one would expect high O_3 associated with local O_3 production to occur during peak O_3 production months (June – October) and specifically to occur near midday associated with peak solar radiance and photochemical production. A shift in the timing of high O_3 events to later in the day would suggest additional influences such as an increased influence of vertical transport, derived from deep mixing of the boundary layer, observed in the

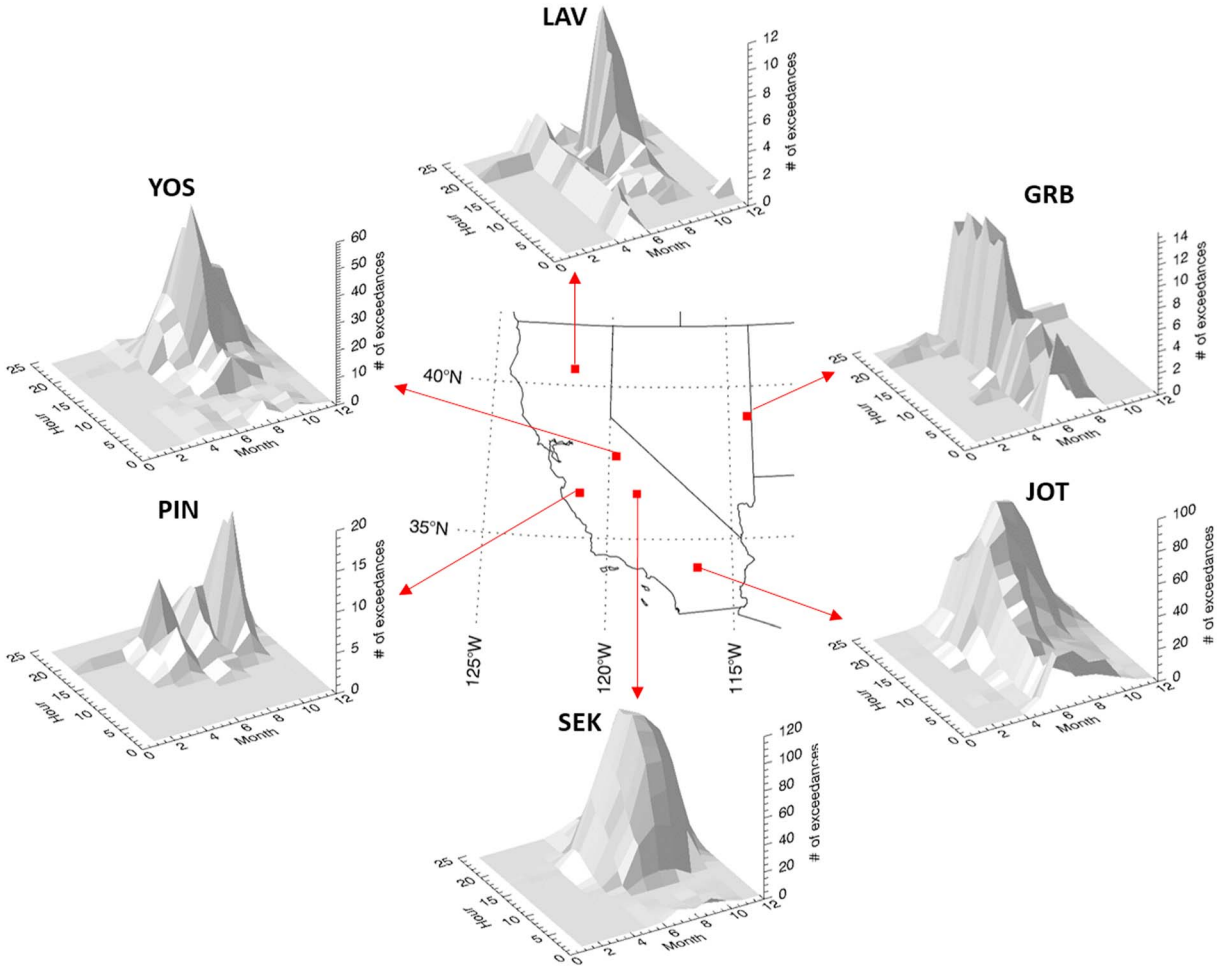

Figure 7. Frequency distributions by month and hour of day for the number of times hourly O_3 mixing ratios exceed 70 ppb during 2010–2014 at Great Basin (GRB, elev. 2,060 m), Joshua Tree (JOT, elev. 1,224 m), Sequoia (SEK, elev. 1,225 m), Pinnacles (PIN, elev. 335 m), Yosemite (YOS, elev. 1,605 m), and Lassen Volcanic (LAV, elev. 1,756 m) National Parks.

late afternoon or early evening (VanCuren, 2015) and regional-scale transport of polluted air (e.g., Burley et al., 2017). Observance of high O_3 events outside of peak O_3-producing months implies an additional causation such as vertical transport of high O_3 from aloft (e.g., UTLS and lofted pollution layers) down into the boundary layer.

From Figure 7, it can be seen that high O_3 events observed at YOS, PIN, and SEK mainly fall within June to November and ~10:00 to 20:00 local time, with peak O_3 events occurring late in the afternoon/early evening. This implies that local photochemical O_3 production combined with vertical transport (boundary layer mixing) plays important roles in controlling O_3 levels at these sites. LAV also shows a similar trend between July and October. However, during April to June LAV experiences high O_3 events that persist within the nocturnal boundary layer. This springtime occurrence implies that O_3 during these months is influenced by vertical transport of elevated O_3 from aloft to the surface. LAV (elev. 1,756 m) has a higher elevation than YOS, PIN, and SEK and as such is more impacted by the free troposphere than are the lower altitude sites. Previous work has documented less pronounced diurnal cycles at high elevation sites due to well-defined nocturnal inversions and smaller local nocturnal NO_x emissions leading to less nighttime O_3 depletion (e.g., Parrish et al., 2010).

JOT (elev. 1,244 m) is at a similar elevation as SEK (elev. 1,225 m) so one would expect a similar pattern of O_3 behavior. However, JOT observes the peak occurrence of high O_3 events earlier in the year and later in the

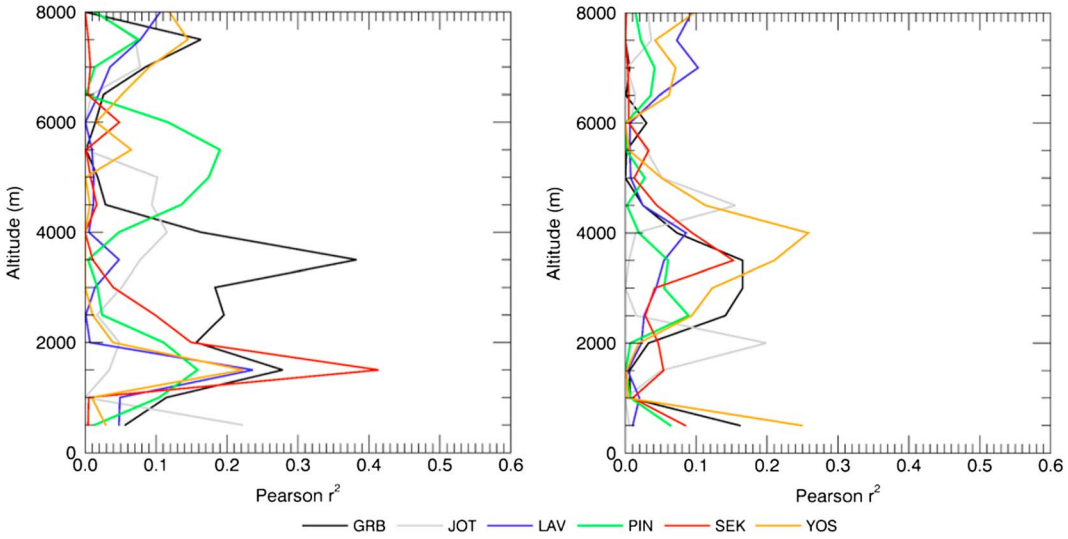

Figure 8. Correlation coefficients of mean AJAX O_3 with seasonally corrected surface O_3 measured at Great Basin (GRB, black), Joshua Tree (JOT, gray), Lassen Volcanic (LAV, blue), Pinnacles (PIN, green), Sequoia (SEK, red), and Yosemite (YOS, orange) National Parks in spring (April–May, left) and summer (June–September, right) 2010–2014.

day than SEK implying that JOT is more heavily impacted by transported O_3 than SEK. During summer months, high O_3 events also persist throughout the night at JOT, unlike SEK. An analysis of how JOT and other O_3 sites in the Mojave Desert are impacted by O_3 transported from the Los Angeles megacity or aloft is presented by VanCuren (2015).

GRB is the site with the highest elevation within this data set (elev. 2,060 m), and high O_3 events are observed from May to September and persist through the day and night. This site seems more impacted by vertical transport than the others in this study, and the impacts of vertical transport (including from the UTLS, entrainment into the boundary layer of previous day's O_3, and lofted (long range and local) pollution layers) are arguably more important than local O_3 production at GRB.

To explore the relationship between surface O_3 and O_3 aloft, correlation analysis between O_3 measured by AJAX and at CASTNET surface sites is presented in Figure 8. Since the surface sites cover a large regional area, we chose to use the regional measurements of AJAX O_3 for the correlation analysis (see Figure 1). We followed the methodology presented by Yates et al. (2015). As an estimator of the seasonal cycle for a given CASTNET site, we calculated the hourly surface O_3 mixing ratio averaged over 29 days, centered on the flight day in question. The 29 day average value at the mean time of a single AJAX flight was then subtracted from the surface-measured hourly O_3, and the difference (surface O_3 − estimated seasonal O_3) was used in the correlation analysis. The correlation (r^2) was calculated between seasonally corrected surface O_3 and the mean regional O_3, averaged in 500 m vertical layers over the entire AJAX flight. Figure 8 presents r^2 as a function of altitude for different sites in spring (left) and summer (right). R^2 can be used to estimate the fraction of the variance of a dependent variable that can be explained by its independent variable (Parrish et al., 2010). Overall, correlations between AJAX observations and surface O_3 are larger in spring than in summer months and are weaker still in winter/fall (not shown). Enhanced correlations suggest there are common influences that impact O_3 at CASTNET surface sites and O_3 aloft.

4. Conclusions and Implications

Reductions in anthropogenic U.S. emissions of O_3 precursors are the likely cause of the decreasing summertime 95th percentile O_3 (high O_3 events) at CASTNET sites analyzed in this study, ranging from −0.47 to −0.88 O_3 ppb yr^{-1} (between June and September 1995–2015). This trend becomes weaker or reverses for the summertime medium and low O_3 events (50th and 5th percentiles). During springtime (April–May, 1995–2015), there are more increasing trends observed than decreasing trends and less statistical significance,

particularly at the 5th percentile, with increases at five sites, ranging from 0.05 to 0.19 O_3 ppb yr^{-1}. This indicates an underlying increase in what is considered baseline O_3 at these EPA-designated clean air sites.

The recent reduction of the U.S. NAAQS O_3 standard from 75 ppb to 70 ppb combined with increasing baseline O_3 impacts the attainment status of O_3 surface sites, with 10 or more exceedances annually at the more polluted sites (JOT, SEK, and YOS). The majority of the additional exceedances as a result of the lowered NAAQS fall within summer months, but some sites also show increased exceedances in spring and fall, seasons not typically associated with peak photochemical O_3 production. As such, observation and identification of the sources (e.g., local or long-range transported pollution or UTLS) of high O_3 events are of increasing importance from a regulatory point of view.

During 2012 there was a notable increase in CASTNET MDA8 O_3 and in the number of exceedance days. GEOS-Chem analysis indicated that these increases may be primarily due to increased UTLS exposure in 2012 (compared to 2013), highlighting the importance and influence of air aloft on surface O_3 values in the western U.S. In spring, 72% of vertical O_3 data (AJAX aircraft, ozonesonde, and lidar) have elevated O_3 laminae, defined as $O_3 > 70$ ppb between 3 and 8 km. In summer, the percentage drops slightly to 65%. The seasonal O_3 cycle between 3 and 8 km has a maximum in April (AJAX and lidar) and May (ozonesonde). Below 3 km, the O_3 seasonal cycle shows more variability due to differences in location and timing of observations, with peaks in April (ozonesonde), August (AJAX), and bimodal with peaks in May and September (lidar). The variability of O_3 values <3 km is indicative of the competing influences on surface O_3 in the western U.S.

The temporal differences observed among high-surface O_3 events at CASTNET sites can be used to assess influencing factors. High O_3 events at PIN, SEK, and YOS primarily occur during summer and fall between 10:00 and 20:00 local time, implying that local photochemical O_3 production combined with vertical transport (boundary layer mixing) play important roles in controlling O_3 levels at these sites. JOT shows peak high O_3 events during spring and later in the day indicating that JOT is strongly impacted by transported O_3. GRB, JOT, and LAV all show high O_3 events that persist through the nocturnal boundary layer, which is not evident in PIN, SEK, and YOS. Correlation analysis of surface O_3 from CASTNET sites and regional O_3 measured by AJAX further supports the hypothesis that free tropospheric air affects surface O_3, with, for example, a third of the variance observed at GRB accounted for by influences common to both surface O_3 and O_3 between 2 and 4 km during spring.

This study provides a detailed observation-based analysis of O_3 over California and Nevada and highlights the importance of considering both surface O_3 and O_3 aloft in the context of increasing baseline O_3 and more stringent air quality standards. Given the challenges of modeling O_3 in the mountainous terrain of the western U.S., this study provides useful insight into the sources of elevated surface O_3 observed in the rural western U.S.

Acknowledgments
The authors gratefully recognize the support and partnership of H211 L.L.C., with particular thanks to K. Ambrose, R. Simone, T. Grundherr, B. Quiambao, J. Lee, and R. Fisher. Funding was provided by the Bay Area Environmental Research Institute, NASA Postdoctoral Program, NASA Ames Research Center Director's funds, and the NASA High-End Computing (HEC) Program through the NASA Advanced Supercomputing (NAS) Division at NASA Ames Research Center. Technical contributions from E. Quigley, M. Loewenstein, and J. Tadić made this project possible. The authors would like to thank D. Jacob and the Harvard University Atmospheric Chemistry Modeling Group for providing the base GEOS-Chem model used during our research. The AJAX data used in this study are available upon request to the corresponding author. The views, opinions, and findings contained in this report are those of the author(s) and should not be construed as an official National Oceanic and Atmospheric Administration or U.S. Government position, policy, or decision.

References

Akagi, S. K., Yokelson, R. J., Burling, I. R., Meinardi, S., Simpson, I., Blake, D. R., … Weise, D. R. (2013). Measurements of reactive trace gases and variable O3 formation rates in some South Carolina biomass burning plumes. *Atmospheric Chemistry and Physics*, *13*, 1141–1165. https://doi.org/10.5194/acp-13-1141-2013

Ambrose, J. L., Reidmiller, D. R., & Jaffe, D. A. (2011). Causes of high O_3 in the lower free troposphere over the Pacific Northwest as observed at the Mount Bachelor Observatory. *Atmospheric Environment*, *45*, 5302–5315. https://doi.org/10.1016/j.atmosenv.2011.06.056

Amos, H. M., Jacob, D. J., Holmes, C. D., Fisher, J. A., Wang, Q., Yantosca, R. M., … Gustin, M. S. (2012). Gas-particle partitioning of atmospheric Hg(II) and its effect on global mercury deposition. *Atmospheric Chemistry and Physics*, *12*, 591–603.

Appenzeller, C., Holton, J. R., & Rosenlof, K. H. (1996). Seasonal variation of mass transport across the tropopause. *Journal of Geophysical Research*, *101*, 15,071–15,078. https://doi.org/10.1029/96JD00821

Baylon, P. M., Jaffe, D. A., Pierce, R. B., & Gustin, M. S. (2016). Interannual variability in baseline ozone and its relationship to surface ozone in the western U.S. *Environmental Science & Technology*, *50*(6), 2994–3001. https://doi.org/10.1021/acs.est.6b00219

Bey, I., Jacob, D. J., Yantosca, R. M., Logan, J. A., Field, B., Fiore, A. M., … Schultz, M. (2001). Global modeling of tropospheric chemistry with assimilated meteorology: Model description and evaluation. *Journal of Geophysical Research*, *106*, 23,073–23,095. https://doi.org/10.1029/2001JD000807

Brodin, M., Helmig, D., & Oltmans, S. (2010). Seasonal ozone behavior along an elevation gradient in the Colorado front range mountains. *Atmospheric Environment*, *44*, 5305–5315. https://doi.org/10.1016/j.atmosenv.2010.06.033

Brown-Steiner, B., & Hess, P. (2011). Asian influence on surface ozone in the United States: A comparison of chemistry, seasonality, and transport mechanisms. *Journal of Geophysical Research*, *116*, D17309. https://doi.org/10.1029/2011JD015846

Burley, D. D., & Ray, J. D. (2007). Surface ozone in Yosemite National Park. *Atmospheric Environment*, *41*, 6048–6062. https://doi.org/10.1016/jatmosenv.2007.03.021

Burley, D. D., Bytnerowicz, A., Buhler, M., Zielinska, B., Schweizer, D., Cisneros, R., … Dulen, D. (2017). Air quality at Devils Postpile National Monument, Sierra Nevada Mountains, California, USA. *Aerosol and Air Quality Research*, *16*(10), 2315–2332. https://doi.org/10.4209/aaqr.2016.02.0069

Burley, D. D., Bytnerowicz, A., Ray, J. D., Schilling, S., & Allen, E. D. (2014). Surface ozone in Joshua Tree National Park. *Atmospheric Environment*, *87*, 95–107. https://doi.org/10.1016/jatmosenv.2013.12.043

Bytnerowicz, A., Tausz, M., Alsonso, R., Jones, D., Johnson, R., & Grulke, N. (2002). Summer-time distribution of air pollutants in Sequoia National Park, California. *Environmental Pollution*, *118*(2), 187–203. https://doi.org/10.1016/S0269-7491(01)00312-8

Cooper, O. R., Parrish, D. D., Stohl, A., Trainer, M., Nédélec, P., Thouret, V., … Avery, M. A. (2010). Increasing springtime ozone mixing ratios in the free troposphere over western North America. *Nature*, *463*. https://doi.org/10.1038/nature08708

Cooper, O. R., Oltmans, S. J., Johnson, B. J., Brioude, J., Angevine, W., Trainer, M., … Stajner, I. (2011). Measurement of western U.S. baseline ozone from the surface to the tropopause and assessment of downwind impact regions. *Journal of Geophysical Research*, *116*, D00V03. https://doi.org/10.1029/2011JD016095

Cooper, O. R., Gaom, R.-S., Tarasick, D., LeBlanc, T., & Sweeney, C. (2012). Long-term ozone trends at rural ozone monitoring sites across the United States, 1990–2010. *Journal of Geophysical Research*, *117*, D22307. https://doi.org/10.1029/2012JD01826

Cooper, O. R., Langford, A. O., Parrish, D. D., & Fahey, D. W. (2015). Challenges of a lowered U.S. ozone standard. *Science*, *348*(6239), 1096–1097. https://doi.org/10.1126/science.aaa5748

Darmenov, A. S., & da Silva, A. (2015). *The Quick Fire Emissions Dataset (QFED): Documentation of versions 2.1, 2.2 and 2.4*. R. D. Koster (Ed.), (Vol. 38). USA.

Fine, R., Miller, M. B., Burley, J., Jaffe, D. A., Pierce, R. B., Lin, M., & Sexauer Gustin, M. (2014). Variability and sources of surface ozone at rural sites in Nevada, USA: Results from two years of the Nevada rural Ozone Initiative. *The Science of the Total Environment*, 530–531. https://doi.org/10.1016/j.scitotenv.2014.12.027

Fiore, A. M., Jacob, D. J., Liu, H., Yantosca, R. M., Fairlie, T. D., & Li, Q. (2003). Variability in surface ozone background over the United States: Implications for air quality policy. *Journal of Geophysical Research*, *108*(D24), 4787. https://doi.org/10.1029/2003JD003855.

Granados-Muñoz, M. J., & Leblanc, T. (2016). Tropospheric ozone seasonal and long-term variability as seen by lidar and surface measurements at the JPL-Table Mountain Facility, California. *Atmospheric Chemistry and Physics*, *16*, 9299–9319. https://doi.org/10.5194/acp-16-9299-2016

Gratz, L. E., Jaffe, D. A., & Hee, J. R. (2015). Causes of increasing ozone and decreasing carbon monoxide in springtime at the Mount Bachelor Observatory from 2004 to 2013. *Atmospheric Environment*, *109*, 323–330. https://doi.org/10.1016/j.atmosenv.2014.05.076

Jaffe, D. A. (2011). Relationship between surface ozone and free tropospheric ozone in the western U.S. *Environmental Science & Technology*, *45*, 432–438. https://doi.org/10.1021/es1028102

Jaffe, D. A., & Widger, N. L. (2012). Ozone production from wildfires: A critical review. *Atmospheric Environment*, *51*, 1–10. https://doi.org/10.1016/j.atmosenv.2011.11.063

Jaffe, D. A., & Zhang, L. (2017). Meteorological anomalies lead to elevated O_3 in the western U.S. in June 2015. *Geophysical Research Letters*, *44*, 1990–1997. https://doi.org/10.1002/2016GL072010

Langford, A. O., Brioude, J., Cooper, O. R., Senff, C. J., Alvarez, R. J. II, Hardesty, R. M., … Oltmans, S. J. (2012). Stratospheric influence on surface ozone in the Los Angeles area during late spring and early summer of 2010. *Journal of Geophysical Research*, *117*, D00V06. https://doi.org/10.1029/2011JD016766

Langford, A. O., Senff, C. J., Alvarez, R. J. II, Brioude, J., Cooper, O. R., Holloway, J. S., … Williams, E. J. (2015). An overview of the 2013 Las Vegas Ozone Study (LVOS): Impact of stratospheric intrusions and long-range transport on surface air quality. *Atmospheric Environment*, *109*, 305–322. https://doi.org/10.1016/j.atmosenv.2014.08.040

Langford, A. O., Alvarez, R. J. II, Brioude, J., Fine, R., Gustin, M. S., Lin, M. Y., … Williams, E. J. (2017). Entrainment of stratospheric air and Asian pollution by the convective boundary layer in the southwestern U.S. *Journal of Geophysical Research: Atmospheres*, *122*, 1312–1337. https://doi.org/10.1002/2016JD025987

Lefohn, A. S., Wernli, H., Shadwick, D., Limbach, S., Oltmans, S. J., & Shapiro, M. (2011). The importance of stratospheric-tropospheric transport in affecting surface O_3 mixing ratios in the western United States. *Atmospheric Environment*, *45*, 4845–4857. https://doi.org/10.1016/j.atmosenv.2011.06.014

Lin, J.-T., & McElroy, M. (2010). Impacts of boundary layer mixing on pollutant vertical profiles in the lower troposphere: Implications to satellite remote sensing. *Atmospheric Environment*, *44*(14), 1726–1739. https://doi.org/10.1016/j.atmosenv.2010.02.009

Lin, M., Fiore, A. M., Horowitz, L. W., Cooper, O. R., Naik, V., Holloway, J., … Wyman, B. (2012). Transport of Asian ozone pollution into surface air over the western United States in spring. *Journal of Geophysical Research*, *117*, D00V07. https://doi.org/10.1029/2011JD016961

Lin, M., Fiore, A. M., Horowitz, L. W., Langford, A. O., Oltmans, S. J., Tarasick, D., & Rieder, H. E. (2015). Climate variability modulates western US ozone air quality in spring via deep stratospheric intrusions. *Nature Communications*, *6*, 7105. https://doi.org/10.1038/ncomms8105

Lin, M., Horowitz, L. W., Cooper, O. R., Tarasick, D., Conley, S., Iraci, L. T., … Yates, E. L. (2015). Revisiting the evidence of increasing springtime ozone mixing ratios in the free troposphere over western North America. *Geophysical Research Letters*, *42*, 8719–8728. https://doi.org/10.1002/2015GL065311

Lin, M., Horowitz, L. W., Payton, R., Fiore, A. M., & Tonnesen, G. (2017). US surface ozone trends and extremes from 1980 to 2014: Quantifying the roles of rising Asian emissions, domestic controls, wildfires and climate. *Atmospheric Chemistry and Physics*, *17*, 2943–2970. https://doi.org/10.5194/acp-17-2943-2017

Lin, S. J., & Rood, R. B. (1996). Multidimensional flux form semi-Lagrangian transport schemes. *Monthly Weather Review*, *124*, 2046–2070. https://doi.org/10.1175/1520-0493(1996)124<2046:MFFSLT>2.0.CO;2

Liu, H., Jacob, D. J., Bey, I., & Yantosca, R. M. (2001). Constraints from 210Pb and 7Be on wet deposition and transport in a global three dimensional chemical tracer model driven by assimilated meteorological fields. *Journal of Geophysical Research*, *106*, 12,109–12,128.

McDermid, I. S., Beyerle, G., Haner, D. A., & Leblanc, T. (2002). Redesign and improved performance of the tropospheric ozone lidar at the Jet Propulsion Laboratory Table Mountain Facility. *Applied Optics*, *41*(36), 7550–7555. https://doi.org/10.1364/AO.007550

McLinden, C. A., Olsen, S. C., Hannegan, B., Wild, O., Prather, M. J., & Sundet, J. (2000). Stratospheric ozone in 3-D models: A simple chemistry and the cross-tropopause flux. *Journal of Geophysical Research*, *105*, 14,653–14,665. https://doi.org/10.1029/2000JD900124

Newchurch, M. J., Ayoub, M. A., Oltmans, S., Johnson, B., & Schmidlin, F. J. (2003). Vertical distribution of ozone at four sites in the United States. *Journal of Geophysical Research*, *108*(D1), 4031. https://doi.org/10.1029/2002JD002059.

Oltmans, S. J., Lefohn, A. S., Harris, J. M., & Shadwick, D. S. (2008). Background ozone levels of air entering the west coast of the US and assessment of longer-term changes. *Atmospheric Environment*, *42*, 6020–6038. https://doi.org/10.1016/j.atmosenv.2008.03.034

Parrish, D. D., Aikin, K. C., Oltmans, S. J., Johnson, B. J., Ives, M., & Sweeny, C. (2010). Impact of transported background ozone inflow on summertime air quality in a California ozone exceedance area. *Atmospheric Chemistry and Physics*, *10*, 10,093–10,109. https://doi.org/10.5194/acp-10-10093-2010

Parrish, D. D., Law, K. S., Staehelin, J., Derwent, R., Cooper, O. R., Tanimoto, H., … Chan, E. (2012). Long-term changes in lower tropospheric baseline ozone concentrations at northern mid-latitudes. *Atmospheric Chemistry and Physics*, *12*, 11,485–11,504. https://doi.org/10.5194/acp-12-11485-2012

Parrish, D. D., Law, K. S., Staehelin, J., Derwent, R., Cooper, O. R., Tanimoto, H., … Chan, E. (2013). Lower tropospheric ozone at northern midlatitudes: Changing seasonal cycle. *Geophysical Research Letters*, *40*, 1631–1636. https://doi.org/10.1002/grl.50303

Pfister, G. G., Wiedinmyer, C., & Emmons, L. K. (2008). Impacts of the fall 2007 California wildfires on surface ozone: Integrating local observations with global model simulations. *Geophysical Research Letters*, *35*, L19814. https://doi.org/10.1029/2008GL034747

Pfister, G. G., Parrish, D. D., Worden, H., Emmons, L. K., Edwards, D. P., Wiedinmyer, C., … Wisthaler, A. (2011). Characterizing summertime chemical boundary conditions for air masses entering the US West Coast. *Atmospheric Chemistry and Physics*, *11*, 1769–1790. https://doi.org/10.5194/acp-11-1769-2011

Ryoo, J.-M., Johson, M. S., Iraci, L. T., Yates, E. L., Pierce, R. B., Tanaka, T., & Gore, W. (2017). Investigating sources of ozone in California using AJAX airborne measurements and models: Implications for stratospheric intrusion and long-range transport. *Atmospheric Environment*, *155*, 53–67. https://doi.org/10.1016/j.atmosenv.2017.02.008

Singh, H. B., Cai, C., Kaduwela, A., Weinheimer, A. J., & Wisthaler, A. (2012). Interactions of fire emissions and urban pollution over California: Ozone formation and air quality simulations. *Atmospheric Environment*, *56*, 45–51.

Škerlak, B., Sprenger, M., & Wernli, H. (2014). A global climatology of stratosphere-troposphere exchange using the ERA-Interim data set from 1979 to 2011. *Atmospheric Chemistry and Physics*, *14*, 913–937. https://doi.org/10.5194/acp-14-913-2014

Travis, K. R., Jacob, D. J., Fisher, J. A., Kim, P. S., Marais, E. A., Zhu, L., … Zhou, X. (2016). Why do models overestimate surface ozone in the Southeast United States?. *Atmospheric Chemistry and Physics*, *16*, 13,561–13,577. https://doi.org/10.5194/acp-16-13561-2016

VanCuren, R. (2015). Transport aloft drives peak ozone in the Mojave Desert. *Atmospheric Environment*, *109*, 331–341. https://doi.org/10.1016/j.atmosenv.2014.09.057

Wang, Y. H., Jacob, D. J., & Logan, J. A. (1998). Global simulation of tropospheric O3-NO_x-hydrocarbon chemistry: 1. Model formulation. *Journal of Geophysical Research*, *103*, 10,713–10,725.

Yates, E. L., Iraci, L. T., Roby, M. C., Pierce, R. B., Johnson, M. S., Reddy, P. J., … Gore, W. (2013). Airborne observations and modeling of springtime stratosphere-to-troposphere transport over California. *Atmospheric Chemistry and Physics*, *13*, 12,481–12,494. https://doi.org/10.5194/acp-13-12481-2013

Yates, E. L., Iraci, L. T., Austerberry, D., Pierce, R. B., Roby, M. C., Tadić, J. M., … Gore, W. (2015). Characterizing the impacts of vertical transport and photochemical ozone production on an exceedance area. *Atmospheric Environment*, *109*, 342–350. https://doi.org/10.1016/j.atmosenv.2014.09.002

Yates, E. L., Iraci, L. T., Singh, H. B., Tanaka, T., Roby, M. C., Hamill, P., … Gore, W. (2016). Airborne measurements and emission estimates of greenhouse gases and other trace constituents from the 2013 California Yosemite Rim wildfire. *Atmospheric Environment*, *127*, 293–302. https://doi.org/10.1016/j.atmosenv.2015.12.038

Zhang, L., Jacob, D. J., Boersma, K. F., Jaffe, D. A., Olson, J. R., Bowman, K. W., … Weinheimer, A. J. (2008). Transpacific transport of ozone air pollution and the effect of recent Asian emission increases on air quality in North America: An integrated analysis using satellite, aircraft, ozonesonde and surface observations. *Atmospheric Chemistry and Physics*, *8*, 6117–6136. https://doi.org/10.5194/acp-8-6117-2008

Zhang, Y., Olsen, S. C., & Dubey, M. K. (2010). WRF/Chem simulated springtime impact of rising Asian emissions on air quality over the U.S. *Atmospheric Environment*, *44*(24), 2799–2812. https://doi.org/10.1016/j.atmosenv.2010.05.003